ORIGINAL RESEARCH

Polydopamine-Coated Kaempferol-Loaded MOF Nanoparticles: A Novel Therapeutic Strategy for Postoperative Neurocognitive Disorder

Enhao Huang[1,2,*], Huadao Li[2,3,*], Hanghang Han [1,2,*], Lianshan Guo [4], Yubing Liang[3], Zijin Huang[1], Ke Qin[5], Xueke Du [1]

[1]Department of Anesthesiology, The Second Affiliated Hospital of Guangxi Medical University, Nanning, Guangxi Zhuang Autonomous Region, 530007, People's Republic of China; [2]Key Laboratory for Basic Science and Prevention of Perioperative Organ Dysfunction, Guangxi Medical University Cancer Hospital, Nanning, Guangxi Zhuang Autonomous Region, 530021, People's Republic of China; [3]Department of Anesthesiology, Guangxi Medical University Cancer Hospital, Nanning, Guangxi Zhuang Autonomous Region, 530021, People's Republic of China; [4]Department of Emergency, The Second Affiliated Hospital of Guangxi Medical University, Nanning, Guangxi Zhuang Autonomous Region, 530007, People's Republic of China; [5]Guilin People's Hospital, Guilin, Guangxi Zhuang Autonomous Region, 541100, People's Republic of China

*These authors contributed equally to this work

Correspondence: Ke Qin; Xueke Du, Email qinke303@163.com; duxueke@gxmu.edu.cn

Purpose: The primary objective of this study was to develop an innovative nanomedicine-based therapeutic strategy to alleviate Postoperative Neurocognitive Disorder (PND) in patients undergoing surgery.

Patients and Methods: To achieve this goal, polydopamine-coated Kaempferol-loaded Metal-Organic Framework nanoparticles (pDA/KAE@ZIF-8) were synthesized and evaluated. The study involved encapsulating Kaempferol (KAE) within ZIF-8 nanoparticles, followed by coating with polydopamine (PDA) to enhance biocompatibility and targeted delivery. The characterization of these nanoparticles (NPs) was conducted using various techniques including Scanning Electron Microscopy, Fourier-Transform Infrared Spectroscopy, X-ray Diffraction, and Ultraviolet-Visible spectroscopy. The efficacy of pDA/KAE@ZIF-8 NPs was tested in both in vitro and in vivo models, specifically focusing on their ability to penetrate the blood-brain barrier and protect neuronal cells against oxidative stress.

Results: The study found that pDA/KAE@ZIF-8 NPs efficiently penetrated the blood-brain barrier and were significantly taken up by neuronal cells. These nanoparticles demonstrated remarkable Reactive Oxygen Species (ROS) scavenging capabilities and stability under physiological conditions. In vitro studies showed that pDA/KAE@ZIF-8 NPs provided protection to HT-22 neuronal cells against H_2O_2-induced oxidative stress, reduced the levels of pro-inflammatory cytokines, and decreased apoptosis rates. In a PND mouse model, the treatment with pDA/KAE@ZIF-8 NPs significantly improved cognitive functions, surpassing the effects of KAE alone. This improvement was substantiated through behavioral tests and a noted reduction in hippocampal inflammation.

Conclusion: The findings from this study underscore the potential of pDA/KAE@ZIF-8 NPs as an effective nanotherapeutic agent for PND. This approach offers a novel direction in the postoperative care of elderly patients, with the potential to transform the therapeutic landscape for neurocognitive disorders following surgery. The application of nanotechnology in this context opens new avenues for more effective and targeted treatments, thereby improving the quality of life for patients suffering from PND.

Keywords: nanomedicine, reactive oxygen species, blood-brain barrier

Introduction

Postoperative cognitive dysfunction (PND) is a significant concern, particularly for elderly patients undergoing surgery. It affects approximately 40% of these patients, manifesting as delirium, confusion, memory loss, attention deficit, and cognitive decline.[1–3] These symptoms not only increase mortality and prolong hospital stays but also detrimentally impact patients' long-term quality of life. Given the growing elderly population and their frequent need for surgery, developing effective strategies for preventing and managing PND is crucial.[4] However, current preventive and treatment options for PND are inadequate, highlighting the urgent need for new approaches.[5]

Recent studies have linked neuroinflammation and oxidative stress to PND.[6–8]Surgical trauma exacerbates this by activating immune cells in the central nervous system, which increases reactive oxygen species (ROS) production and inflammatory factor secretion, contributing to neuroinflammation.[9–11] Furthermore, neuronal cell death is a key factor in cognitive decline. Addressing this, the clearance of ROS through medication to protect brain neurons is emerging as a promising strategy for PND management.[12–14]

In this context, plant-derived drugs, particularly flavonoids like Kaempferol (KAE), are gaining attention for their anti-inflammatory and antioxidant properties.[15,16] KAE, a natural flavonoid, is effective in scavenging ROS and maintaining antioxidant enzyme activity. It also intervenes in neurodegenerative diseases by crossing the blood-brain barrier (BBB) and modulating microglia-mediated neuroinflammation, downregulating inflammatory factors such as IL-6 and TNF-α, thereby protecting neurons.[17,18] Increasing evidence suggests that KAE has unique advantages in neuroprotection, but its low solubility and absorption efficiency lead to poor bioavailability in the body. Furthermore, KAE is easily affected by metabolic processes in the body, although it performs excellently in in vitro cellular models, but its performance in vivo is less satisfactory. Therefore, ensuring that KAE can smoothly penetrate the BBBand target inflammation sites, prolong its half-life in the body, and improve its bioavailability and therapeutic effects is a major challenge currently faced by natural compound medications. In this context, nanomedicine technology offers an effective solution to the challenges faced by KAE in treating brain diseases. Utilizing nanomedicine technology to construct drug carriers for KAE not only improves drug stability, prolongs the half-life, facilitates its crossing of the BBB, but also enhances targeting and therapeutic efficiency. This strategy can not only break through biological barriers to achieve precise drug delivery but also enhance the therapeutic effects of the drug, reduce side effects, and increase the controllability and predictability of treatment, promising new breakthroughs in the treatment of brain diseases. Metal-Organic Frameworks (MOFs) like ZIF-8, known for their unique porous structure and pH responsiveness, are ideal for drug delivery due to their high surface area and stability.[19,20] Our study introduces ZIF-8 nanoparticles (NPs) loaded with KAE and surface-modified with polydopamine (PDA), creating the pDA/KAE@ZIF-8 NPs. Dopamine's ability to self-polymerize, forming a PDA layer on various materials, coupled with PDA's ROS scavenging abilities, enhances the antioxidant effects of these nanoparticles.[21] This nanomedicine system offers good biocompatibility, enhanced passive targeting, pH responsiveness, and potential for synergistic PND treatment. The aim of this study is to assess the efficacy of pDA/KAE@ZIF-8 NPs in preventing and treating PND. It seeks not only to enhance the effectiveness of KAE but also to pioneer new treatment directions for PND. In summary, this study strives to develop innovative drug delivery systems and shift the current PND treatment paradigm, with the goal of providing more effective treatment options for patients.

Materials and Methods

Synthesis of pDA/KAE@ZIF-8

Initially, KAE (MB2171,Meilunbio) was dissolved in a DMSO solution, and 0.3633 g of $Zn(NO_3)_2 \cdot 6H_2O$ was dissolved in 100 mL of methanol. Then, 1.626 g of 2-methylimidazole was dissolved in another 100 mL of methanol, and this mixture was combined with the previous one. The combined solution was stirred at room temperature for 12 hours, followed by high-speed centrifugation (10,000 rpm for 10 minutes) and triple washing with methanol to eliminate unreacted reagents, successfully yielding KAE@ZIF-8 NPs. Subsequent steps involved adding 1 mg of dopamine hydrochloride to 20 mL of Tris-HCl buffer (10 mM, pH 8.5), then introducing 4 mg of the prepared KAE@ZIF-8 NPs into this solution. The mixture was stirred for 2 hours in a light-protected environment, continuously monitoring the pH. The resulting black turbid solution was centrifuged for 10 minutes at 10,000 rpm to obtain pDA/KAE@ZIF-8 NPs. These were then washed, freeze-dried, and stored at −20 °C.

The Characterization of pDA/KAE@ZIF-8

Scanning Electron Microscopy (SEM, Hitachi SU8020, 5 KV) was used to analyze the morphology of ZIF-8 and pDA/KAE@ZIF-8. Particle size and Zeta potential were assessed using Zetasizer Nano ZS90, and the crystalline structure of the nanoparticles was determined by X-ray powder diffraction (XRD, D8 ADVANCE X-ray diffractometer). Fourier-transform infrared spectroscopy (FTIR, Nicolet 6700) analyzed the chemical functional groups on the nanoparticle surfaces, while UV-Vis-NIR spectroscopy (UV, UV-3600 spectrophotometer) was used for absorption spectrum analysis. Finally, the nanoparticles' suspension stability was determined by measuring their size in PBS and DMEM solutions over 0–14 days.

Evaluation of KAE Drug Release

A study was conducted where in 1 mg of pDA/KAE@ZIF-8 was dispersed in 10 mL of phosphate-buffered saline (PBS) at pH values of either 5.5 or 7.4. After stirring and agitation, 1 mL of the supernatant was collected at predetermined time intervals and replenished with an equivalent volume of PBS. This process was repeated thrice, and the concentration of KAE was subsequently calculated using a spectrophotometer.

EPR Spectroscopy Analysis of ROS Scavenging Ability

pDA/KAE@ZIF-8 NPs (concentration of 100 µg/mL) were introduced into solutions containing $^{\bullet}OH$ or $^{\bullet}O_2^{-}$ free radicals and H_2O_2, and incubated at room temperature for 30 minutes. Then, 5.5-dimethyl-1-pyrroline N-oxide (DMPO) was added as a scavenger and incubation continued for an additional 10 minutes. The scavenging abilities of pDA/KAE@ZIF-8 against $^{\bullet}OH$ and $^{\bullet}O_2^{-}$ free radicals, as well as H_2O_2, were detected using an electron paramagnetic resonance spectrometer (A300-10/12).

In Vitro BBB Assessment

The BBB model was established in vitro using the transwell method, co-culturing human brain microvascular endothelial cells (HBMEC) and hippocampal neuron cells (HT-22). Following previous studies,[22] HBMECs were cultured in the upper chamber at a density of 3×10^5 cells until the trans-endothelial electrical resistance reached 330 ohm·cm^2. Subsequently, HT-22 cells were planted in the lower chamber to establish the BBB model. After adding pDA/KAE@ZIF-8 to the upper chamber, samples were collected from the lower chamber after 24 hours, centrifuged to obtain the supernatant, and their absorbance was measured. The permeability rate was calculated as (Concentration of nanomaterials in the lower chamber / Initial concentration of nanomaterials in the upper chamber) × 100%.

Cell Culture and Cytotoxicity Evaluation

HBMEC cells and HT-22 cells were procured from Wuhan Puno Sai Life Science Technology Co., Ltd. The culture medium used was DMEM containing 10% fetal bovine serum, supplemented with penicillin and streptomycin to form a complete culture medium. The cells were incubated in a 37 °C, 5% CO_2 incubator until they reached 80% confluency for passaging. HT-22 cells (4×10^4 per well) were planted in a 96-well plate. After cell adhesion, different concentrations of drugs were added to each well and incubated for 48 hours. Cell viability was assessed using the CCK8 method. The cytotoxicity and damage reversal of pDA/KAE@ZIF-8 on HT-22 cells induced by H_2O_2 were also evaluated using CCK8. After cell adhesion, different concentrations of pDA/KAE@ZIF-8 were incubated for 12 hours, with the control group treated with an equivalent volume of PBS. H_2O_2 solution (100 µM) was then added and incubated for 2 hours. Absorbance at 450 nm wavelength was measured using an enzyme marker.

Intracellular Uptake of pDA/KAE@ZIF-8

During the preparation of pDA/KAE@ZIF-8, Cy5.5 was selected as a fluorescent marker. Fluorescence microscopy was employed to observe and measure the intracellular uptake of pDA/KAE@ZIF-8 in HT-22 cells. Briefly, HT-22 cells were seeded in a 24-well plate at a density of 4×10^4 cells. After cell adhesion, the cells were incubated with Cy5.5-labeled pDA/KAE@ZIF-8 for various durations. The culture medium was discarded, and the cells were washed three times with PBS to remove external particles. Finally, DAPI staining was added, and fluorescence was observed under a fluorescence microscope.

Reactive Oxygen Species (ROS) Staining

The detection of ROS in cells was performed using 2',7'-dichlorofluorescein diacetate (DCFH-DA) as a fluorescent probe. Cells from different treatment groups were incubated in DCFH-DA-containing blank DMEM (without FBS) for 30 minutes at 37 °C and 5% CO_2 in a light-protected environment. After washing with PBS, the intensity of green fluorescence, proportional to the intracellular ROS levels, was observed under a fluorescence microscope. We then further explored the ROS scavenging ability of NPs by flow cytometry.

Nitrogen-Free Radical (DPPH•) Scavenging Assay

Referring to the relevant literature,[23] briefly, different concentrations of pDA/KAE@ZIF-8 NPs were added to the pre-configured solution. React for 30 min at 37 °C, protected from light. Determine the absorbance of the supernatant at 520 nm. PBS was used as a blank group. DPPH•-clearance was calculated based on absorbance changes as follows (Ab: absorbance of blank group, As: absorbance of material group).

$$Scavenging\ ratio(\%) = \frac{Ab - As}{Ab} \times 100\%$$

Flow Cytometry

Flow cytometry was used to assess the impact of pDA/KAE@ZIF-8 on cell apoptosis. In brief, cells from different treatment groups were double-stained using an Annexin V/FITC kit (Vazyme). Apoptotic cells were marked with Annexin V and FITC, and then analyzed using a BDTMLSRII flow cytometer to determine the proportion of apoptotic cells.

Calcein-AM Staining

Cell viability was determined using the Calcein-AM staining method. After experimental treatment, HT-22 cells were washed twice with PBS. Then, the cells were incubated with Calcein-AM (Invitrogen, USA) in PBS at 37 °C in the dark for 30 minutes. Post-incubation, the culture dishes were washed with PBS to remove excess dye, and fluorescence images were captured under a fluorescence microscope.

Assessment of Mitochondrial Membrane Potential (Δψm) with JC-1 Staining

Mitochondrial membrane potential was evaluated using JC-1 staining. Cells were seeded at a density of 3×10^4 cells/well in a 24-well plate and treated according to experimental conditions. After treatment, cells were washed with PBS and stained with 10 μg/mL JC-1 dye (Beyotime, China) at 37 °C for 20 minutes. Following incubation, cells were washed twice with PBS, and observations were made under a fluorescence microscope.

Animal and PND Model

A total of 32 male C57BL/6 mice, procured from the Experimental Animal Center of Guangxi Medical University, were raised to the age of eight months. They were provided with adequate food and water, maintained in a 12-hour light/dark cycle, at a temperature of 21–26 °C, and a relative humidity of about 50%. The ethical review of animal experiments followed the Guiding Opinions on the Humane Treatment of Laboratory Animals issued by the Ministry of Science and Technology of the People's Republic of China, and the National Standard GB/T35892-2018, which is titled Ethical Standards for Animal Welfare in Experimental Research. The ethical approval for this experiment was granted by The Animal Care & Welfare Committee of Guangxi Medical University. (Approval No: 202,301,100). The mice were randomly divided into four groups (n = 8 each): a sham surgery group, where abdominal skin was incised and treated with saline; a PND group, which received saline treatment post-model establishment; a KAE treatment group, treated with KAE (10 mg/kg, intraperitoneally) for seven days post-model establishment; and a pDA/KAE@ZIF-8 treatment group, receiving pDA/KAE@ZIF-8 treatment for the same duration. The PND model was established as described in the literature, with intraperitoneal administration of 1% pentobarbital sodium (50 mg/kg) for anesthesia, followed by abdominal exploratory surgery. After a week of treatment, behavioral experiments were conducted on the mice, collecting hippocampal tissues and right heart blood, and the animal specimens were stored in a −80 °C freezer.

Open Field Test (OFT)

The open field test apparatus consisted of a 40×40×50 cm square box, with a defined central area measuring 20×20 cm and the remaining area as the periphery. Mice were adapted to the open field box for 5 minutes a day before the start of the experiment. Each mouse was placed from a fixed side and its trajectory was recorded over a 5-minute test period. The test was conducted in a quiet environment with no significant light changes. After each test, the apparatus was cleaned

with 75% ethanol to remove odors. The total distance traveled by the mice and the time spent exploring the central area were recorded using Smart 3.0 software.

Novel Object Recognition Test (NOR)

Two new objects were placed in the open field test box, and mice were allowed to adapt for 5 minutes before the start of the experiment. The next day, one of the objects was replaced with a completely different one, and the mice were allowed to explore freely for 5 minutes, with the time spent exploring the new and old objects recorded. The objects' positions were then changed, and the mice were allowed to explore for another 5 minutes. The Cognitive Index (CI) was calculated as Time exploring the new object / (Time exploring the new object + Time exploring the old object).

Morris Water Maze (MWM) Test

The Morris Water Maze consisted of an elliptical pool (160 cm in diameter and 50 cm high), divided into four quadrants (I, II, III, and IV). A platform (5 cm in diameter) was placed in the center of the third quadrant. The pool was filled with water made opaque with non-toxic ink, and the temperature was maintained at 24 ± 1 °C. Low-level markers were placed around the pool to aid the mice in navigation. Mice had a maximum of 60 seconds to find the platform. If successful, they were allowed to stay on the platform for 10 seconds before being returned to their home cage. If they did not find the platform within 60 seconds, they were guided to it and allowed to stay for 10 seconds. The mice underwent five days of training, with Smart 3.0 software recording the time and distance each mouse took to find the platform area during the training period.

Western Blot

Hippocampal tissues from the treated mice were collected and lysed using RIPA lysis buffer containing protease inhibitors. The tissue proteins were extracted following the protocol provided with the reagent and stored at −20 °C. Protein samples (6 μL per lane) were separated on SDS-PAGE gels and transferred to PVDF membranes. The membranes were then blocked at room temperature for one hour and incubated overnight at 4 °C with primary antibodies against IL-6, IL-1β, and TNF-α. Following incubation, the membranes were treated with secondary antibodies at room temperature for one hour and washed three times with TBST before membrane scanning.

Immunofluorescence

After the MWM experiment, mice were anesthetized with 1% pentobarbital saline, and their abdomens were incised to perform perfusion through the left ventricle with saline, followed by 4% paraformaldehyde. The brain tissues were immediately extracted and soaked in 4% paraformaldehyde for 24 hours, then dehydrated using 30% and 40% sucrose solutions. After dehydration, the tissue sections were embedded, cut into slices approximately 18 μm thick, and blocked with 2% bovine serum albumin, 0.2% TritonX-100, and 5% fetal bovine serum for one hour. The sections were then incubated with primary antibodies for two hours on a shaker, washed three times with PBS, incubated with corresponding secondary antibodies for one hour, washed again, and finally stained with DAPI. Fluorescence microscopy was used to capture the images. The procedure for HT-22 cell fluorescence was similar to tissue immunofluorescence, with 1×10^4 cells seeded in a 24-well plate and stained after adhesion. The antibodies used were Iba-1 (abcam, 1:200), GFAP (abcam, 1:200), Neun (abcam, 1:200), IL-1β (bioss, 1:50), IL-6 (bioss, 1:50), TNF-α (bioss, 1:50), and Goat Anti-Rabbit IgG Secondary Antibody AF488 Conjugated (L3016).

Quantitative q-PCR

Cells were treated according to different group conditions and harvested post-incubation using trypsin without EDTA. Total RNA was extracted from the HT-22 cells using TRIzol reagent as per the kit's instructions. RNA concentration and purity were measured, with standard A260/A280 values between 1.00–2.00. Each RNA sample (1 μg) was reverse-transcribed to cDNA, followed by PCR amplification using primers synthesized by Sangon Biotech (Shanghai) Co., Ltd. The following primers were used: β-actin forward, 5′-GTGCTATGTTGCTCTAGACTTCG-3′; β-actin reverse, 5′-ATGCCACAGGATTCCATACC-3′; IL-6 forward, 5′-TGATGGATGCTACCAAACTGGA-3′; IL-6 reverse, 5′-TGTGACTCCAGCTTATCTCTTG-3′; IL-1β

forward, 5′-ATGCCACCTTTTGACAGTGATG-3′; IL-1β reverse, 5′-TGATGTGCTGCTGCGAGATT-3′; TNF-α forward, 5′-CCCTCACACTCACAAACCAC-3′; TNF-α reverse, 5′-ACAAGGTACAACCCATCGGC-3′.

ELISA for Cell Inflammatory Cytokines

Following different treatment protocols, HT-22 cell culture media were collected and stored at −20 °C. Using ELISA kits, the levels of IL-1β, IL-6, and TNF-α in the cell supernatants were measured according to the instructions provided with the kits.

Hematoxylin and Eosin (H&E) and Nissl Staining

After the completion of the MWM test, the brains were fixed with 4% paraformaldehyde. The brains were then embedded in paraffin and sectioned into slices. The slices underwent deparaffinization and hydration through decreasing ethanol concentrations. To study the histopathological changes in the mice, the sections were stained with H&E and Nissl staining, and observed under a microscope.

Biosafety Evaluation

Two groups of mice were selected, one receiving normal treatment and the other undergoing a 15-day intervention with NPs injections. Blood was first collected from the heart and mixed with a 2% erythrocyte suspension prepared using a glass rod, removing fibrin. According to the protocol, 2% erythrocyte suspension, PBS, and test liquid were added, with PBS serving as the negative control and purified water as the positive control. The mixture was then incubated at 37 °C ±0.5 °C in a water bath. After 3 hours, hemolysis and coagulation reactions were observed, and the hemolysis rate was calculated. Subsequently, routine blood tests and liver and kidney function tests were performed on both groups of mice, along with H&E staining of heart, liver, spleen, lung, kidney, and brain tissues to further verify the biosafety of the NPs.

Network Pharmacology Target Prediction and Molecular Docking
Active Component Screening and Target Prediction

Using the TCMSP database (http://tcmspw.com/tcmsp.php), " Kaempfero l" was searched, selecting components with an oral bioavailability (OB value) ≥ 30% and drug-likeness (DL value) ≥ 0.18.[24] The effective targets of KAE were collected. These targets were then standardized using the Uniprot database (https://www.uniprot.org/).

PND Target Acquisition

PND-related datasets (GSE95426) were downloaded from the GEO database, and differential gene screening, heatmaps, and volcano plots were constructed using R packages. Additionally, disease target databases including Disgenet (https://www.disgenet.org), OMIM (https://www.omim.org), PharmGKB (https://www.pharmgkb.org), Drugbank (https://go.drugbank.com), and Genecards (https://www.genecards.org) were used. The term "postoperative neurocognitive disorder" was used as a keyword to filter targets, and duplicates were removed. The ethical review and declaration of compliance of the database studies related to this study were approved by the Ethical Review Committee of the Second Hospital of Guangxi Medical University (Approval number: 2023-KY(0908)). The use of these databases was conducted in accordance with guidelines and policies governing the ethical use of human-related data in scientific research, ensuring privacy, confidentiality, and security of the data.

Construction of a "Drug-Active Component-Target" Visualization Network

Cytoscape 3.9.1 software was utilized to build a "Component-Target" visualization network diagram with the screened component-drug target data.

PPI Network Construction and Core Target Screening for Drug-Disease Common Targets

The intersecting grid of the screened active components of KAE and PND-related disease targets was generated using Venny 2.1.0. This grid data was imported into the String network platform to determine target interactions (confidence level 0.700), and a PPI network was drawn. Furthermore, network topology analysis of the component-target data was conducted using Cytoscape 3.9.1, and core target genes were selected based on node connectivity, betweenness centrality, and closeness centrality values.

Functional Enrichment Analysis of Intersection Targets

The DAVID (http://david.ncifcrf.gov/) data platform was used for gene ontology (GO) enrichment analysis and the Encyclopedia of Genes and Genomes (KEGG) enrichment analysis of the selected target proteins. The results, including the top-ranking biological processes (BP), molecular functions (MF), cellular components (CC), and signaling pathways, were presented in bar and bubble chart formats, revealing the biological functions and pathways involved in PND potential targets.

Molecular Docking

Core target genes and corresponding components were organized, selecting the final ligands and receptors for pairing. Core components' 2D structure files were obtained from the PubChem (https://pubchem.ncbi.nlm.nih.gov/) database, and their energy was minimized using Chemoffice 3D software. The 3D structures of core protein genes were retrieved from the RCSB PDB database (http://www.rcsb.org/) and processed in PyMOL software to remove small molecules and bound ligand molecules. Molecular docking operations for ligands and receptors were performed using AutoDockTools1.5.7. The binding capabilities between core components and related targets were evaluated, considering a binding energy less than -5 kcal·mol^{-1} as the standard. The greater the absolute value of the binding energy, the stronger the binding capability between the protein and target.

Statistical Analysis

Statistical analysis was conducted using GraphPad Prism 9 software. All data were expressed as mean ± standard deviation. Differences between groups were analyzed using one-way ANOVA and Dunnett's t-test, with *$p < 0.05$, **$p < 0.01$, and ***$p < 0.001$ considered statistically significant.

Results

Characterization of pDA/KAE@ZIF-8 NPs

Figure 1 presents the synthetic strategy of pDA/KAE@ZIF-8 NPs and their mechanism in addressing PND. SEM images in Figures 2A and 2Bi, ii compare ZIF-8 and pDA/KAE@ZIF-8, highlighting their unique morphological features. ZIF-8 NPs are characterized by sharply defined rhombic dodecahedron shapes, averaging around 95 nm in diameter (Figure 2Aiii). In contrast, the pDA/KAE@ZIF-8 NPs exhibit spherical shapes with distinct surface textures.[25] Their average diameter increases to approximately 180 nm (Figure 2 Biii), indicating the successful addition of the PDA shell.
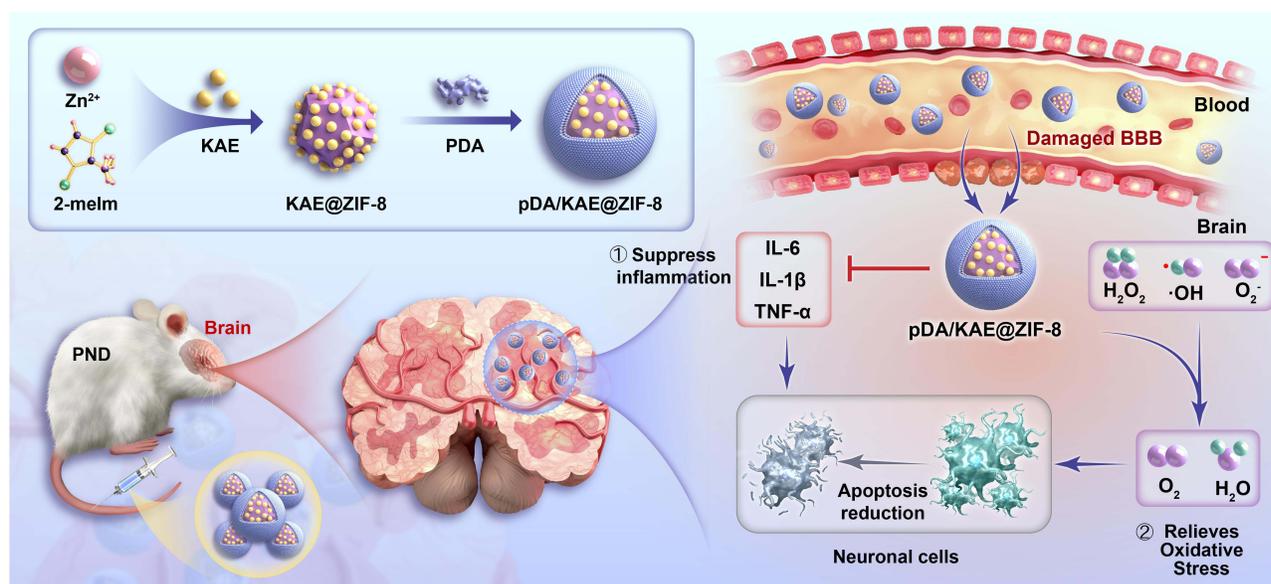

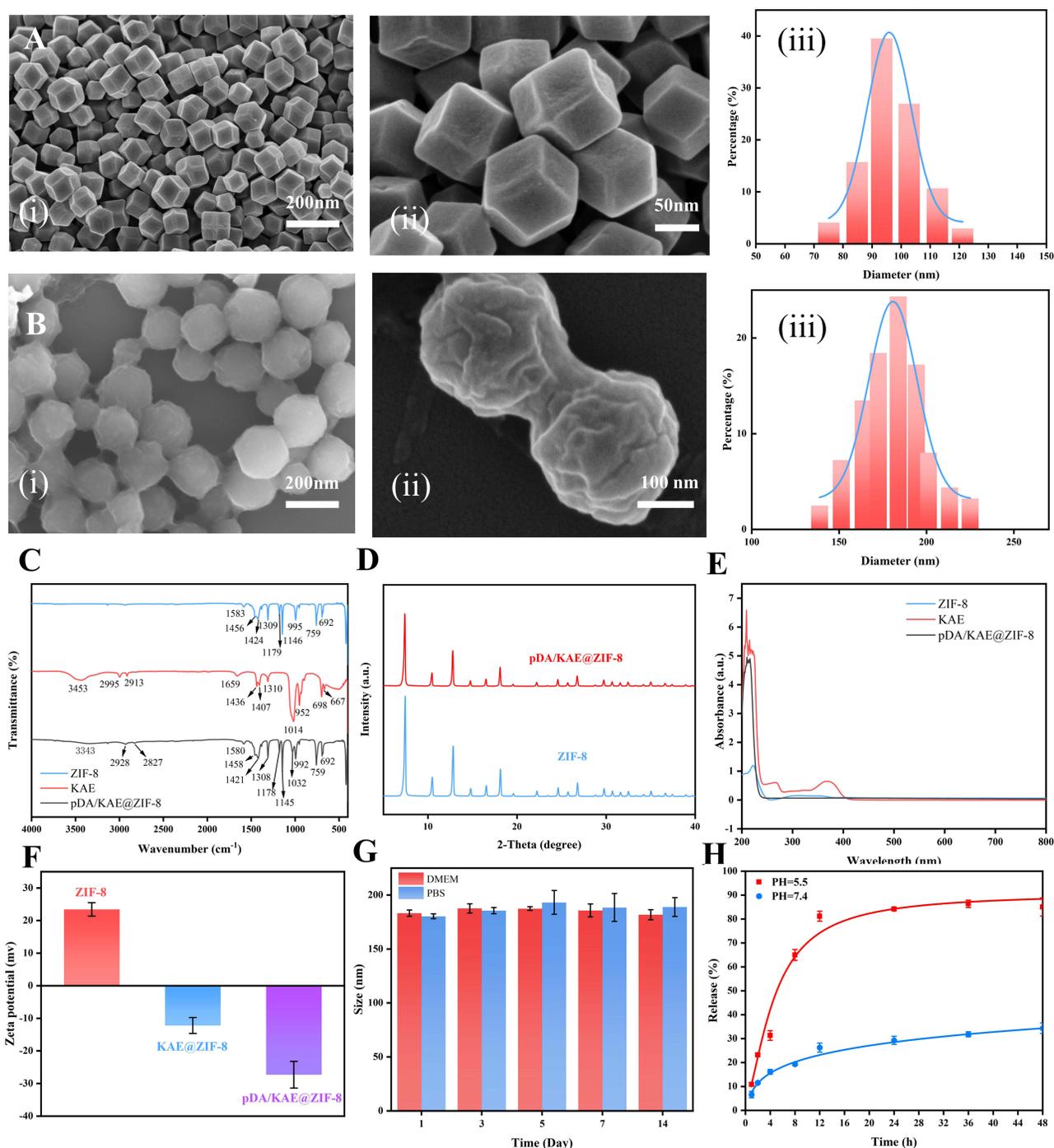**Figure 1** Synthesis and Mechanism of Action of pDA/KAE@ZIF-8 NPs.

Figure 2 Characterization of pDA/KAE@ZIF-8. (**A**) SEM images of ZIF-8 (i, ii) with the average diameter of ZIF-8 depicted (iii). (**B**) SEM images of pDA/KAE@ZIF-8 NPs at various magnifications (i, ii), with the average diameter of pDA/KAE@ZIF-8 NPs presented (iii). (**C**) Infrared spectra of ZIF-8 NPs, KAE, and pDA/KAE@ZIF-8 NPs. (**D**) XRD patterns of ZIF-8 and pDA/KAE@ZIF-8. (**E**) UV-Vis spectra of ZIF-8 NPs, KAE, and pDA/KAE@ZIF-8 NPs. (**F**) Zeta potential measurements of ZIF-8 NPs, KAE, and pDA/KAE@ZIF-8 NPs. (**G**) Suspension stability of pDA/KAE@ZIF-8 NPs in DMEM and PBS solutions. (**H**) Release profiles of KAE from pDA/KAE@ZIF-8 NPs under various pH conditions.

The FTIR spectrum (Figure 2C) identifies characteristic peaks for ZIF-8, KAE, and pDA/KAE@ZIF-8. The spectrum of pDA/KAE@ZIF-8 displays peaks at 3453 cm^{-1}, indicating O-H (PDA and KAE) and N-H (PDA) stretching vibrations. Other notable peaks include 2928 cm^{-1} and 2827 cm^{-1} for C-H stretching, 1503 cm^{-1} and 1458 cm^{-1} for benzene ring vibrations, 1424 cm^{-1} for -CH$_2$- bending, 1308 cm^{-1} for C-N and C-O stretching, and several peaks between 1178 cm^{-1} and 1032 cm^{-1} for C-H in-plane bending. Additionally, peaks at 992 cm^{-1}, 759 cm^{-1}, and 692 cm^{-1} are observed for C-H out-of-plane bending vibrations. These findings confirm KAE and PDA functionalities in pDA/KAE@ZIF-8 NPs.

The XRD pattern in Figure 2D demonstrates the maintained crystal integrity of ZIF-8 within pDA/KAE@ZIF-8 NPs. Meanwhile, the UV-Vis spectrum (Figure 2E) clarifies optical properties. The UV absorption spectrum of KAE shows two strong bands: Band II at 370 nm from cinnamoyl groups ($\pi \rightarrow \pi^*$ transitions) and Band I at 270 nm from benzoyl groups ($n \rightarrow \pi^*$ transitions). Notably, the UV spectrum of pDA/KAE@ZIF-8 lacks kaempferol's characteristic peaks, suggesting its complete encapsulation within the ZIF-8 shell.

Finally, the zeta potential results in Figure 2F highlight a significant charge shift in ZIF-8 NPs. Initially positive, the charge becomes negative with KAE loading and further increases in negativity after PDA shell encapsulation. This shift indicates successful PDA and KAE incorporation, altering surface charge characteristics. These changes are crucial for the nanoparticles' stability, dispersibility, and biological interactions. The reduced positive charge potentially enhances biocompatibility in drug delivery systems, reducing nonspecific cellular adsorption and improving targeting efficiency.[26]

Loading and Release of KAE

In the study of pDA/KAE@ZIF-8 NPs, the focus shifted to the loading and release efficiency of KAE. The encapsulation efficiency (EE%) for KAE was determined to be 39.67%, with a drug loading (DL%) of 21.63%. These values reflect a high efficiency of ZIF-8 NPs in loading KAE. Furthermore, given the pH-responsive nature of ZIF-8, we examined the storage stability and release behavior of pDA/KAE@ZIF-8 NPs. During a 14 day period, these nanoparticles maintained excellent suspension stability in both PBS and DMEM solutions, as shown in Figure 2G.

For assessing KAE release, timed sampling was conducted in solutions replicating physiological conditions. Utilizing the standard curve of KAE (Figure S1), we chose pH levels of 5.5 and 7.4 to investigate release dynamics and calculate the release rates. The findings, depicted in Figure 2H, reveal a significant variance in release rates based on pH levels. At an acidic pH of 5.5, there was an 80% release of KAE within the first 12 hours. Conversely, in a neutral pH 7.4 solution, only 25% of the drug was released over 48 hours. This differential release pattern underscores the efficacy of pDA/KAE@ZIF-8 NPs in targeted drug delivery. Specifically, at inflamed sites characterized by acidic conditions, the nanoparticles efficiently release KAE, thus exerting anti-inflammatory and antioxidative effects.

Penetration of pDA/KAE@ZIF-8 NPs Through the BBB and Cellular Uptake

The HT-22 cell line, derived from mouse hippocampal neurons, serves as a model for neurodegenerative diseases research. Using this cell line, we established an H_2O_2-induced damage model to examine the protective effects of pDA/KAE@ZIF-8 against oxidative stress in HT-22 cells. Initially, the viability of HT-22 cells exposed to various concentrations of pDA/KAE@ZIF-8 NPs for 48 hours was assessed. According to the findings in Figure 3A, the materials, in concentrations ranging from 0 to 64 μg/mL, displayed no significant cytotoxicity. For inducing cellular damage, a 100 μM H_2O_2 solution was selected based on literature references. Treatment with different concentrations of pDA/KAE@ZIF-8 NPs was applied to counteract this damage. Our observations, as depicted in Figure 3B, revealed that all concentrations of pDA/KAE@ZIF-8 NPs exerted a protective effect, with 16 μg/mL being the most effective dose. This concentration was subsequently selected as the optimal therapeutic dose for further cell experiments.

This section focuses on assessing the capacity of pDA/KAE@ZIF-8 NPs for crossing theBBB and their cellular uptake within the brain. The ability to penetrate the BBB is essential for evaluating the potential of drugs targeting neurological disorders. To this end, an in vitro BBB model was established, as shown in Figure 3C, to simulate the penetration capabilities of pDA/KAE@ZIF-8 NPs through the BBB. The results indicated that at a nanoparticle concentration of 8 μg/mL, the drug demonstrated optimal BBB penetration (Figure S2).

Further investigations were conducted using Cy5.5-labeled pDA/KAE@ZIF-8 NPs to track their uptake by HT-22 cells. As depicted in Figure 3D, the uptake was observed to be time-dependent. This finding is significant as it suggests that during conditions characterized by excessive ROS-induced neuroinflammation and ongoing BBB damage, the nanoparticles can effectively cross the BBB. Once inside the brain, they are absorbed by the cells, potentially offering therapeutic benefits. This observation underscores the potential of pDA/KAE@ZIF-8 NPs in delivering drugs to the brain, particularly in contexts of neurological inflammation and damage.
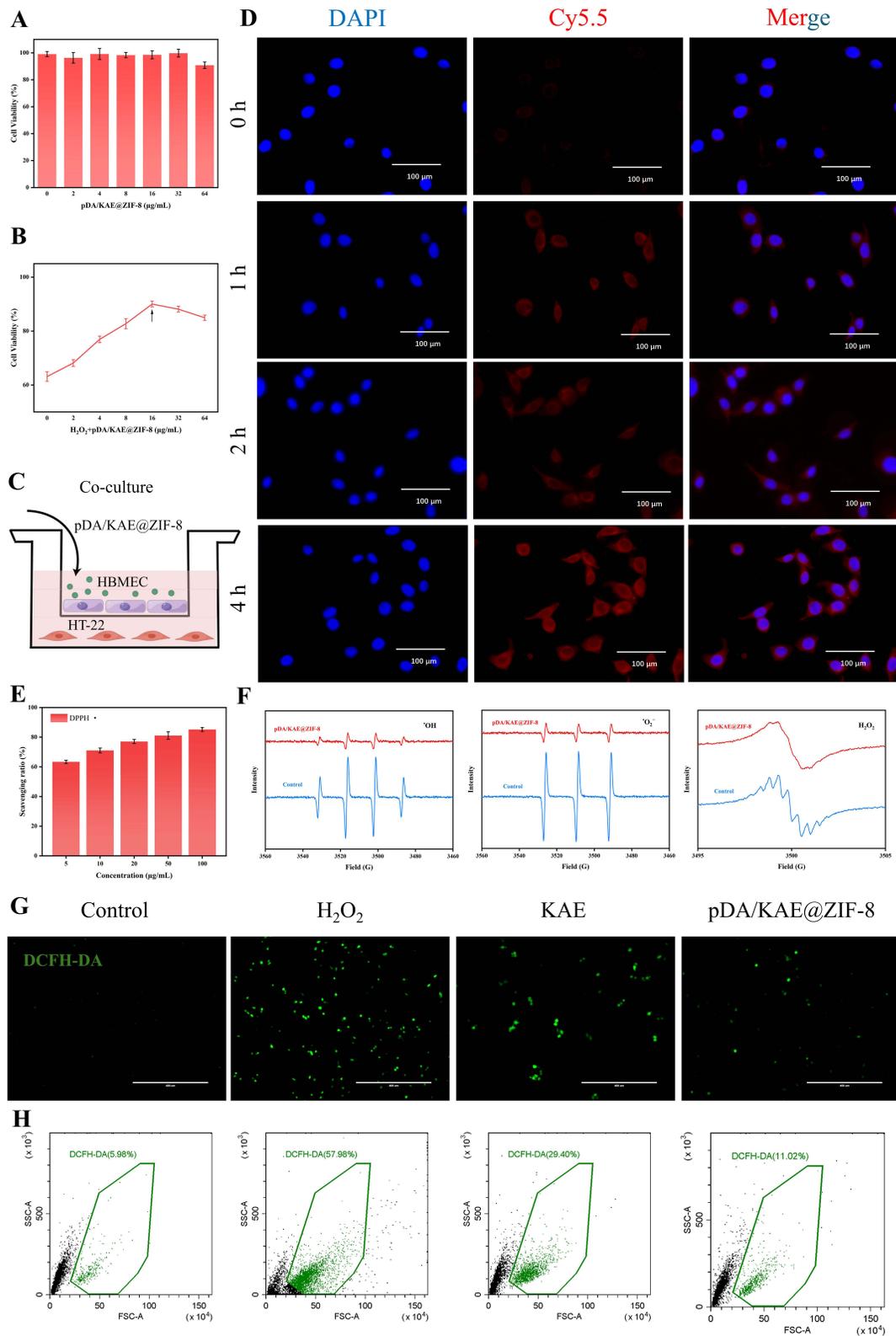
Figure 3 In Vitro Uptake and Antioxidant Capacity of pDA/KAE@ZIF-8 NPs. (**A**) Cell viability of HT-22 cells incubated with varying concentrations of NPs. (**B**) Determination of the optimal incubation concentration through CCK-8 assay under H_2O_2 induction. (**C**) In vitro co-culture model of HT-22 and HBMEC cells. (**D**) Uptake of Cy5.5-labeled pDA/KAE@ZIF-8 NPs by HT-22 cells at different time points. (**E**) pDA/KAE@ZIF-8 NPs DPPH• scavenging capacity. (**F**) EPR spectroscopic analysis of the role of •OH, •O_2^- and H_2O_2 scavenging by pDA/KAE@ZIF-8 NPs. (**G**) In vitro ROS scavenging fluorescence results of pDA/KAE@ZIF-8 NPs. (**H**) Flow cytometric results of the in vitro ROS scavenging effect of pDA/KAE@ZIF-8 NPs.

Protection of HT-22 Cells from Oxidative Stress-Induced Damage by pDA/KAE@ZIF-8

The antioxidant capacity of pDA/KAE@ZIF-8 Nps was tested by DPPH• scavenging assay, as shown in Figure 3E. When the concentration of NPs reached 100 μg/mL, the scavenging efficiency could reach 80%. In addition by confirming the in vitro ROS scavenging capabilities of pDA/KAE@ZIF-8 through EPR spectroscopy, as shown in Figure 3F. The results demonstrated that pDA/KAE@ZIF-8 NPs efficiently cleared H_2O_2, $^{\bullet}O_2^-$, and $^{\bullet}OH^-$ radicals, outperforming the control group.

Intracellular ROS levels were monitored using DCFHDA probes (Figures 3G and H). The results showed that pDA/KAE@ZIF-8 NPs significantly reduced ROS levels induced by H_2O_2, compared to KAE treatment alone. Furthermore, ELISA and qPCR analyses indicated elevated levels of pro-inflammatory mediators (TNF-α, IL-6, IL-1β) post H_2O_2 stimulation (Figure S3). However, treatment with pDA/KAE@ZIF-8 NPs and KAE effectively suppressed these mediators, with statistical significance ($p<0.05$). It's noteworthy that no substantial advantage of pDA/KAE@ZIF-8 NPs over KAE alone was observed at the cellular level. This finding suggests a limitation of the in vitro model, where the targeting benefits of nanoparticles may not be as pronounced as they would be in vivo.

pDA/KAE@ZIF-8 NPs Reduce H_2O_2-Induced Apoptosis in HT-22 Cells

In this study, the Annexin V/FITC kit was employed to determine the rate of apoptosis in HT-22 cells subjected to H_2O_2 and treated with pDA/KAE@ZIF-8 NPs. Flow cytometry results indicated a significant increase in apoptosis among hippocampal neurons after exposure to H_2O_2, with rates reaching approximately 50%. Treatment with KAE managed to reduce this rate to 30.52%, whereas pDA/KAE@ZIF-8 NPs were more effective, bringing it down to 17.77%, as shown in Figure 4A. Notably, this protective effect was predominantly observed in the later stages of apoptosis, with minimal influence on early apoptosis stages (Figure 4B).
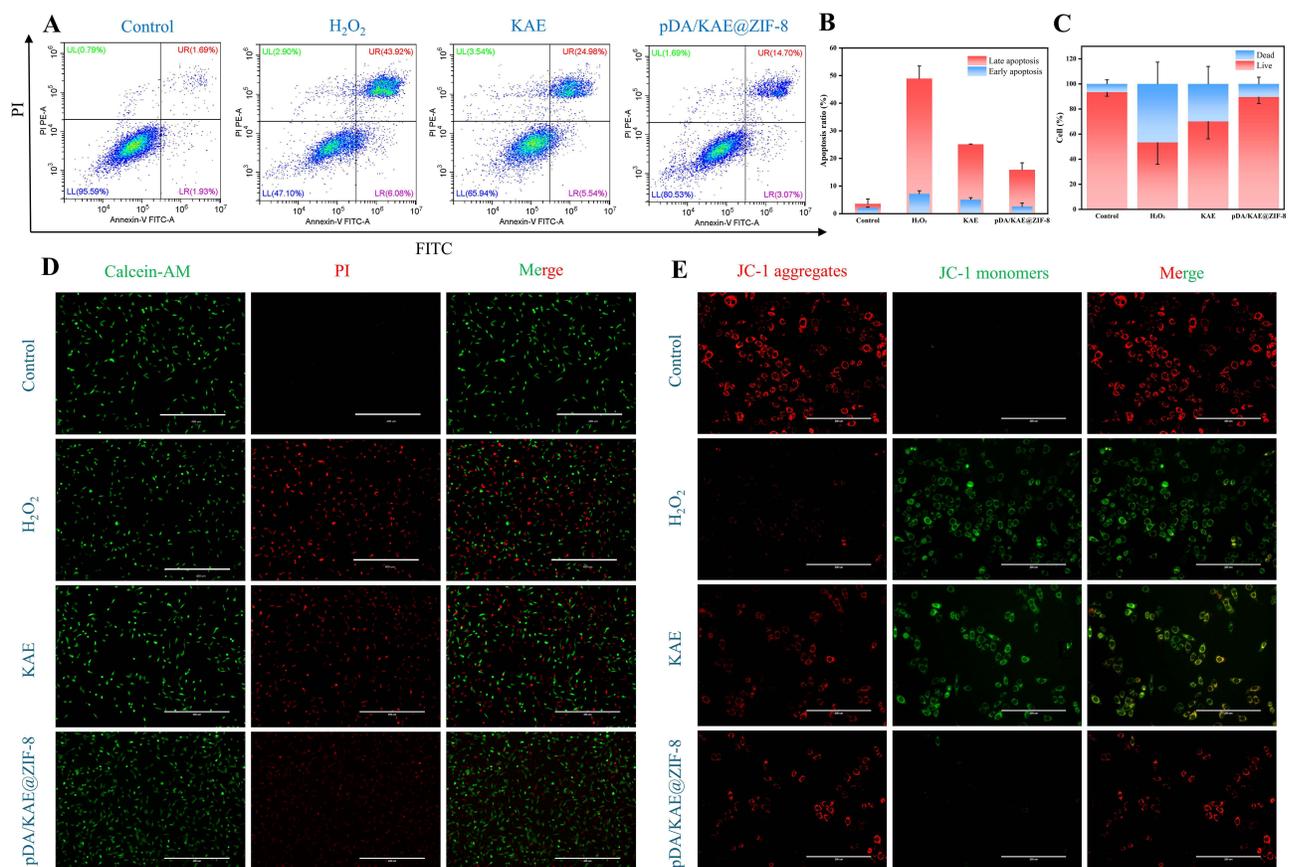

Figure 4 pDA/KAE@ZIF-8 NPs Rescue HT-22 Cells from H_2O_2-Induced Apoptosis. (**A**) Flow cytometry analysis demonstrates the rescuing effect of pDA/KAE@ZIF-8 NPs on H_2O_2-induced apoptosis in HT-22 cells. (**B**) Quantification of the protective effects of pDA/KAE@ZIF-8 NPs against early and late apoptosis induced by H_2O_2 in HT-22 cells. (**C**) Quantitative analysis of Calcein-AM and PI staining .(**D**) Calcein-AM and PI staining. (**E**) JC-1 assay of mitochondrial membrane potential after various treatments.

Additional experiments involving Calcein-AM staining and JC-1 mitochondrial membrane potential assays were conducted. These revealed that H_2O_2 treatment markedly increased apoptotic activity in HT-22 cells compared to the control group. Conversely, cells treated with pDA/KAE@ZIF-8 NPs exhibited a significant reduction in apoptotic numbers (Figures 4C-D) demonstrated restored mitochondrial membrane potential (Figure 4E). In these respects, pDA/KAE@ZIF-8 NPs proved more effective than KAE alone.

Overall, the findings underscore that pDA/KAE@ZIF-8 NPs possess the capacity to significantly mitigate H_2O_2-induced apoptosis in HT-22 cells. Their therapeutic efficacy in reducing cell death and restoring cellular function surpasses that of KAE treatment alone, highlighting their potential as a more effective therapeutic agent.

pDA/KAE@ZIF-8 NPs Improve Cognitive Deficits in PND Mice

In our study, following the experimental timeline outlined in Figure 5A, we developed a PND mouse model and implemented grouped treatments. Initially, to assess differences in motor skills among the groups, we analyzed exploration time and total distance traveled in the central area during a 5-minute free exploration phase. According to the findings presented in Figures 5B and D, there were no significant differences in exploratory behavior or motor abilities among the groups.
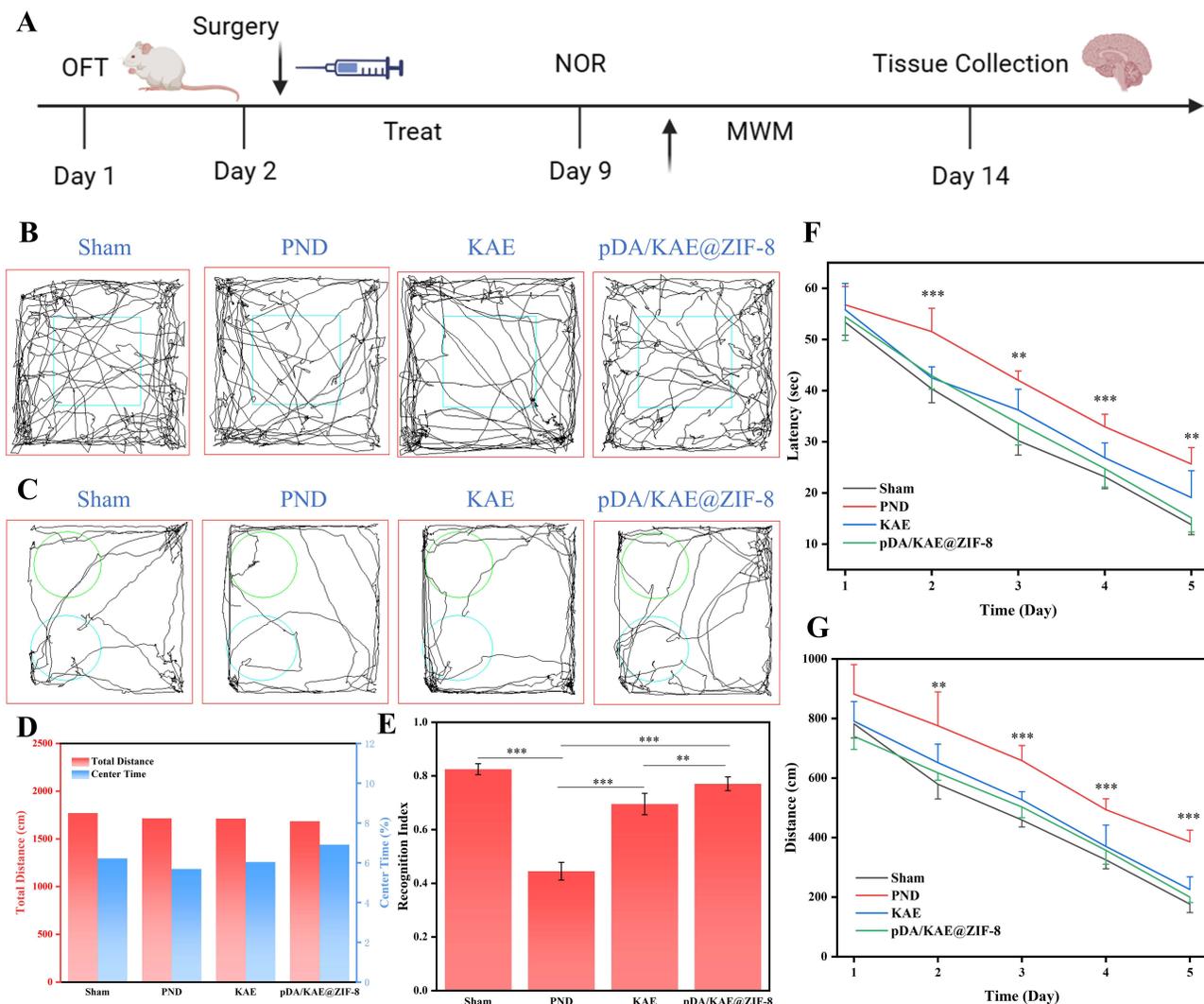

Figure 5 pDA/KAE@ZIF-8 NPs Ameliorate Cognitive Deficits in PND Mice. (**A**) Timeline of behavioral experiments. (**B**) Open field test. (**C**) Novel object recognition test. (**D**) Quantification of travel distance and activity time in the central area during the open field test for different treatment groups. (**E**) Quantification of cognitive indices in the novel object recognition test for different treatment groups. (**F, G**) Training performance over a 5-day period in the Morris water maze test for different treatment groups. ****P < 0.01,***P < 0.001.**

Post-modeling, the mice underwent a week-long treatment regimen. Upon completion of this treatment, a novel object recognition test was conducted. The results, as shown in Figures 5C and E, revealed that the cognitive performance of the PND model mice post-surgery was notably inferior to that of both the sham surgery and treatment groups. This was evident in their decreased exploration time and diminished interest in new objects. The Recognition Index (RI) displayed statistically significant differences ($p < 0.05$), confirming the successful creation of the PND mouse model. Notably, after a week of treatment, the cognitive deficits observed in PND mice were significantly ameliorated. The pDA/KAE@ZIF-8 NPs treatment notably enhanced exploration of new environments and increased exploration time for new objects, outperforming KAE treatment alone.

Moreover, the MWM test, a widely recognized method for assessing cognitive dysfunction in rodents,[27] was employed. As detailed in Figure 5F and G and Figure S4, all mice showed a decrease in escape latency over the five-day training, indicative of successful learning and memory training. Compared to the sham surgery group, the PND mice demonstrated clear cognitive deficits, marked by longer latency periods and increased travel distances, which showed minimal improvement post-training. However, these cognitive impairments were effectively alleviated following treatment with pDA/KAE@ZIF-8 NPs. This treatment led to reduced latency periods and shorter travel distances, with significant improvements ($p < 0.05$) over KAE treatment alone.

In conclusion, the PND mouse model was successfully established, and more importantly, the study demonstrated that pDA/KAE@ZIF-8 NPs treatment significantly enhanced cognitive function in PND mice, surpassing the efficacy of KAE treatment alone.

pDA/KAE@ZIF-8 NPs Alleviate Postoperative Hippocampal Neuroinflammation in Mice

Our research first aimed to determine if pDA/KAE@ZIF-8 NPs could effectively target inflammation sites in vivo. We employed fluorescence detection of Cy5.5-labeled NPs for this purpose. Compared to the control group, a significant increase in red fluorescence intensity at inflammation sites was observed, as depicted in Figure 6A. Additionally, fluorescence images co-stained with the astrocyte marker GFAP (Figure 6B) revealed that Cy5.5-pDA/KAE@ZIF-8 NPs were engulfed and concentrated at these sites, effectively releasing their payload.

Nissl staining, used to evaluate neuronal damage, supported these findings (Figure 6C). Post-treatment, neuron number and arrangement in the CA1, CA3, and DG regions improved, with pDA/KAE@ZIF-8 NPs showing superior results compared to KAE treatment. Further investigation was conducted through H&E staining of hippocampal tissues from different groups, illustrated in Figure 6D and Figure S5. In the sham surgery group, hippocampal neurons displayed regular morphology, denoted by blue arrows, with dense arrangement, large nuclei showing uniform light blue or blue coloration, and clear nucleoli. Contrastingly, in the hippocampal CA3 region of the PND model group, neurons exhibited shrunken nuclei (black arrows), distorted cell bodies, irregular shapes, and blurred nuclear-cytoplasmic boundaries. Remarkably, these adverse changes were mitigated following treatment with pDA/KAE@ZIF-8 NPs, as evidenced by a decrease in neurons with shrunken nuclei and minimal inflammatory cell infiltration.

Under physiological conditions, microglia remain in a resting state, but in disease states, they rapidly activate, as seen in neurodegenerative diseases.[28] In our study, immunofluorescence staining for the microglial marker Iba1 indicated increased expression in the PND group, suggesting activation. This activation was significantly reduced following treatment (Figure 6E).

NeuN, a neuronal biomarker, was also analyzed. The number of neurons and NeuN expression in PND mice were significantly lower compared to the sham surgery group. However, these parameters improved with treatment, particularly with pDA/KAE@ZIF-8 NPs, which outperformed KAE alone (Figure 6F). Western blot analysis of hippocampal tissues (Figure 7A) revealed that the expression of TNF-α, IL-6, and IL-1β was elevated in the PND group, which improved after treatment and was superior to that of KAE treatment alone, demonstrating the superior anti-inflammatory effect of NPs, which was additionally confirmed by the tissue immunofluorescence results as well Figures 7B-D.

In summary, pDA/KAE@ZIF-8 NPs, as a novel nanomedicine delivery system, have shown remarkable therapeutic potential in alleviating neuroinflammation and protecting neurons in PND models.
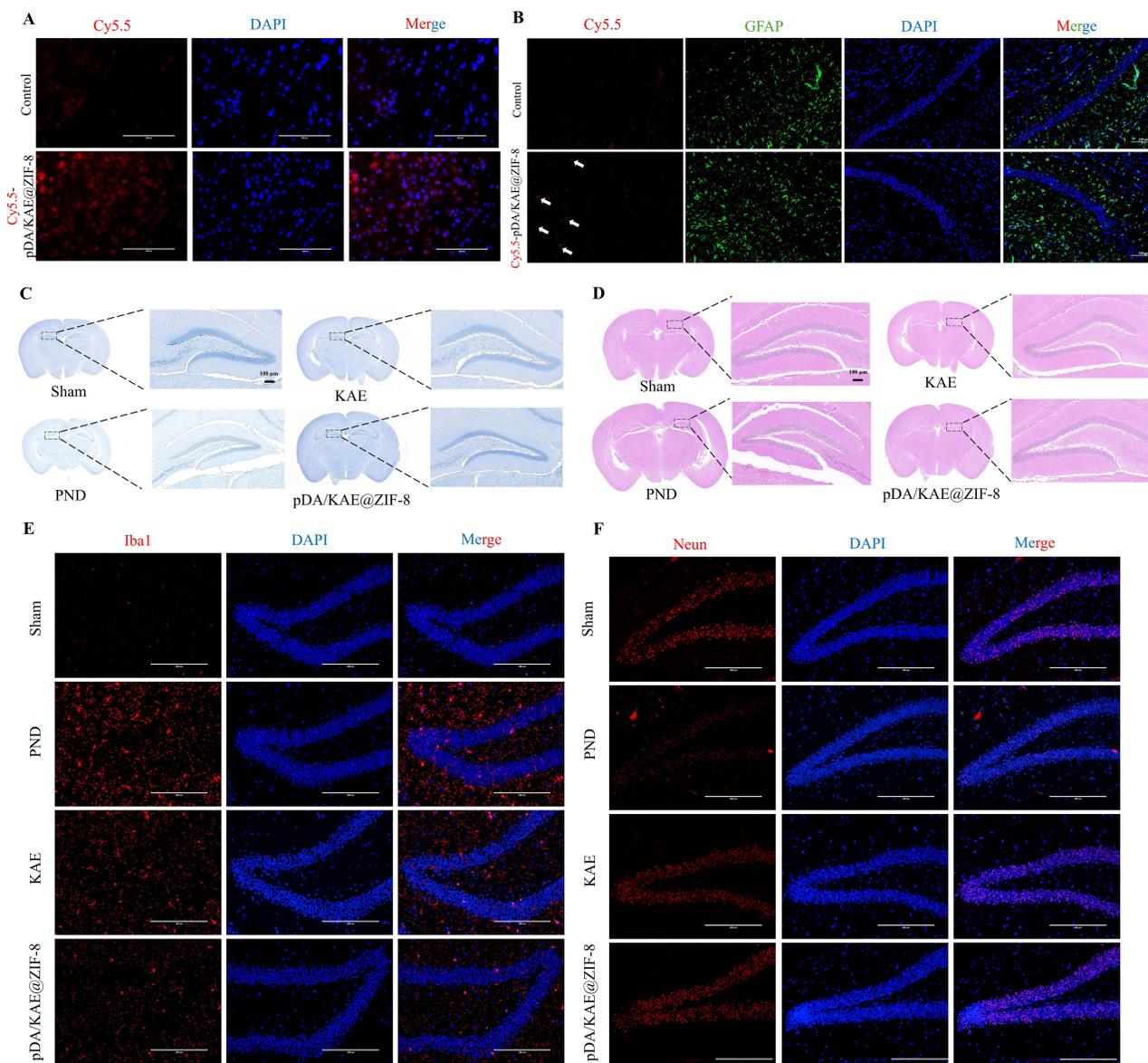
Figure 6 pDA/KAE@ZIF-8 NPs act on the brain inflammation site to reduce the occurrence of neuroinflammation. (**A**) Uptake of cy5.5-pDA/KAE@ZIF-8 at hippocampal inflammation sites. (**B**) Co-staining of cy5.5-pDA/KAE@ZIF-8 NPs with GFAP. (**C** and **D**) Nissl and H&E staining of mice from different treatment groups. (**E**) Immunofluorescent staining for the microglial marker Iba1. (**F**) Immunofluorescent staining for the neuronal marker NeuN.

Network Pharmacology Reveals KAE's Pharmacological Mechanisms in PND Prevention and Treatment

As shown in Figure 8A, to further explore the pharmacological mechanisms of KAE in PND prevention and treatment, we conducted network pharmacology predictive analysis. Against the complex background of PND disease, we constructed a drug-disease common target PPI network and screened for core targets, conducting GO and KEGG analysis on intersecting targets, and finally, validated the network pharmacology conclusions through molecular docking. Initially, we filtered PND-related targets using the GEO database (Figures S6 and 7) and disease target databases such as OMIM, Drug Bank, Disgenet, Pharmgkb, and Genecards, yielding 943 results. We then drew a Venn diagram of PND disease targets (Figure S8), followed by a Venn diagram of drug components-disease targets (Figure S9). Using the gathered target information, we imported it into the String website, obtaining a PPI network relationship diagram of target proteins (Figure S10). In the Degree algorithm diagram (Figure S11), the larger and redder the circle, the more likely it is a key target for treating PND. Subsequent GO and
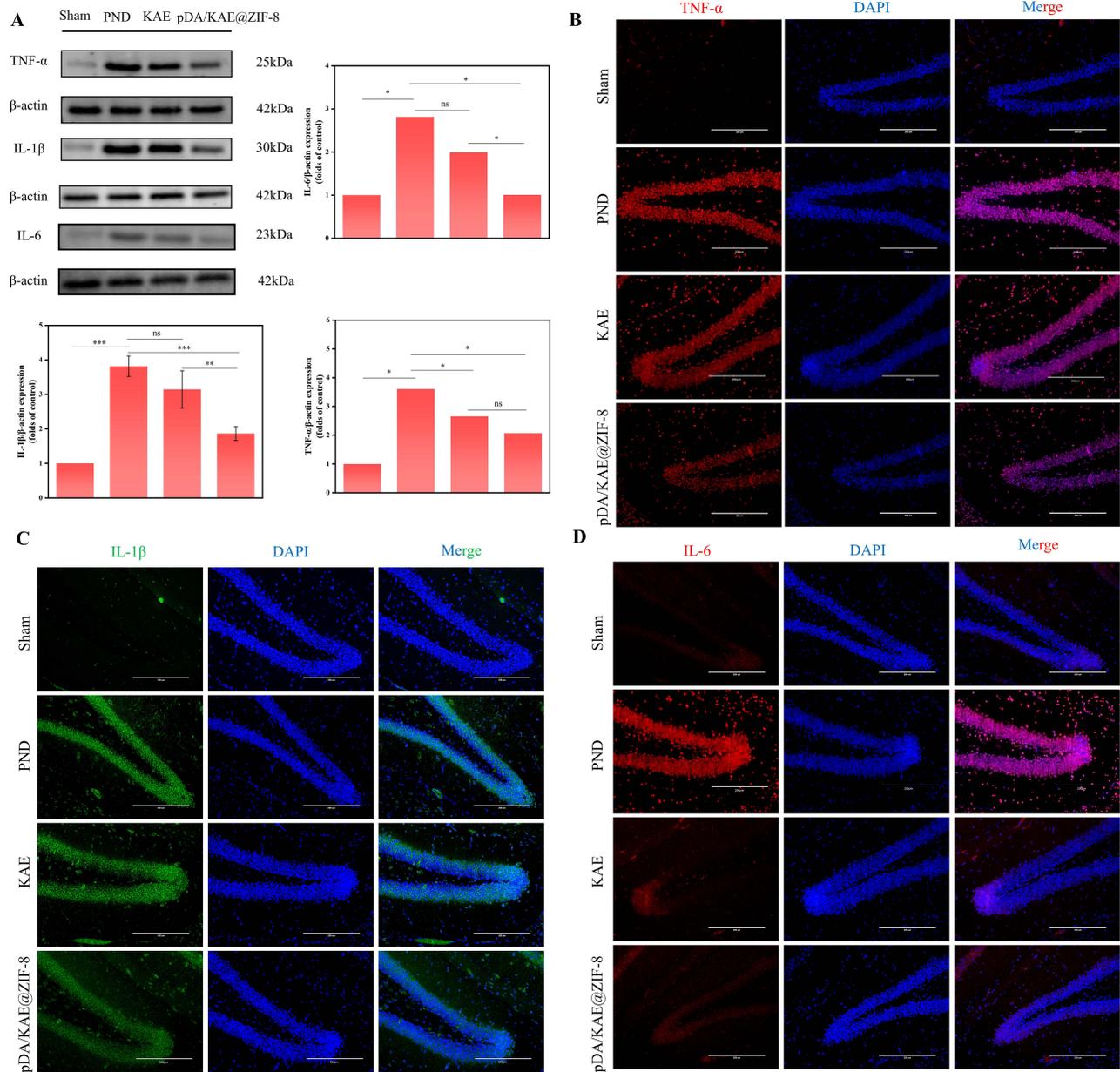
Figure 7 pDA/KAE@ZIF-8 NP treatment attenuates inflammatory factor expression secretion in mice. (**A**) Western blot analysis and quantification of inflammatory factors in hippocampal tissues of mice from different treatment groups. (**B-D**) Immunofluorescent staining of hippocampal tissue mediators TNF-α, IL-1β, and IL-6 across treatment groups. ns means not significant. *P<0.05, **P < 0.01 and ***P < 0.001.

KEGG analysis of the selected Hub targets (Figures 8B and C) suggested that KAE's mechanism in preventing and treating PND might mainly involve the AGE-RAGE signaling pathway, TNF-α signaling pathway, and Apoptosis, with relationships between target proteins and related pathways as shown (Figure 8D). Finally, semi-flexible docking was performed using AutoDock vina on core components and final targets. A total of six molecular docking sessions were conducted. Based on the docking results, the selected targets and components showed good binding activity (Figures 8E and F). Molecular docking results, where grey dashed lines represent hydrophobic interactions between molecules, yellow dashed lines represent hydrogen bonds, and orange dashed lines represent cation-π conjugation, preliminarily confirmed the conclusions of network pharmacology.
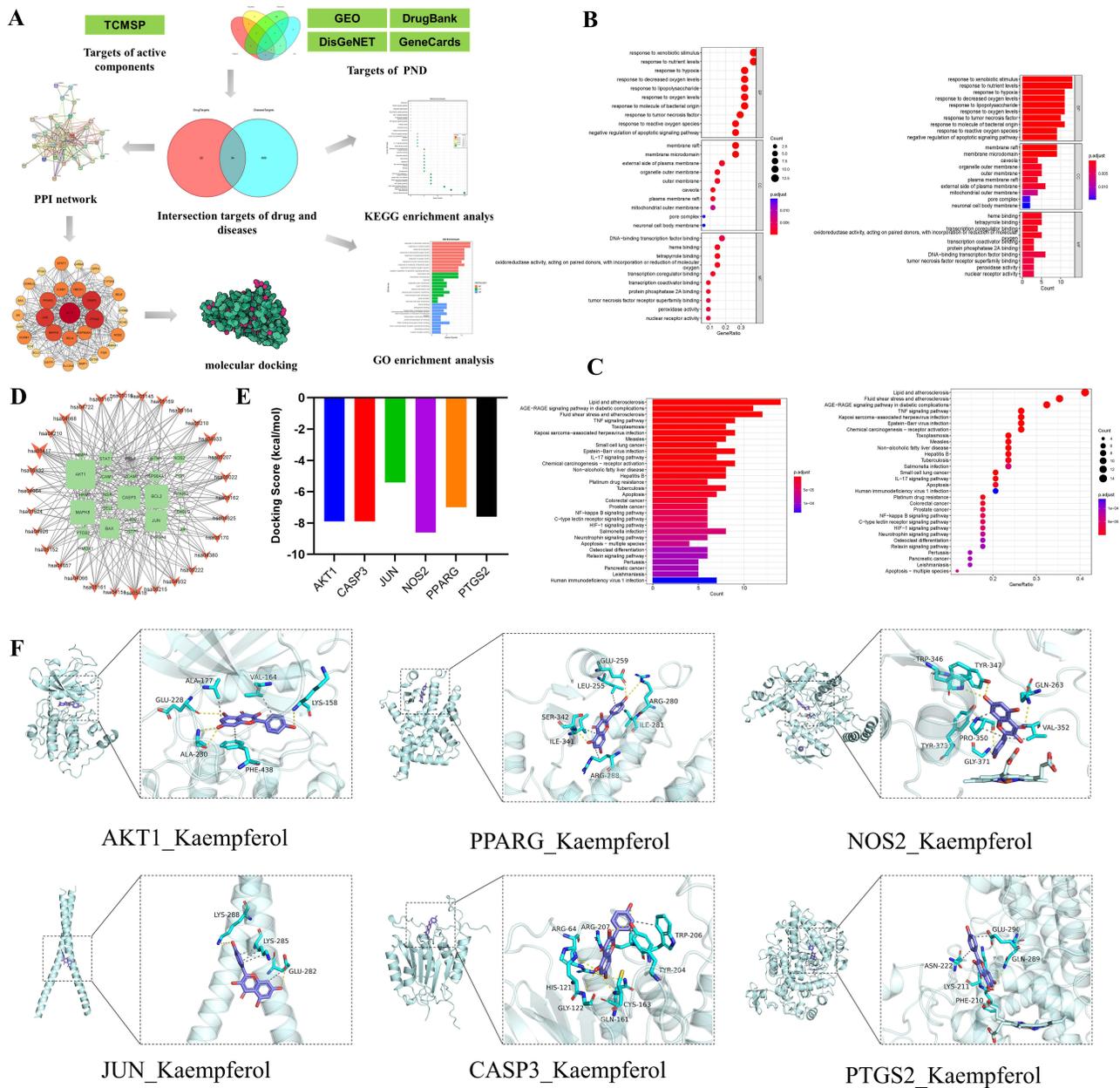
Figure 8 Network Pharmacology Exploration of KAE's Mechanism in the Prevention and Treatment of PND. (**A**) Schematic illustration of network pharmacology for exploring the mechanism of KAE in the prevention and treatment of PND. (**B**) Bubble and bar charts for Gene Ontology (GO) enrichment analysis. (**C**) Bubble and bar charts for KEGG enrichment analysis. (**D**) Schematic interaction diagram of hub genes with related KEGG pathways in the prevention and treatment of PND. (**E**) Heatmap of binding energies between hub genes and KAE molecules. (**F**) Schematic representation of molecular docking between hub genes and KAE molecules.

The Biocompatibility of pDA/KAE@ZIF-8 NPs in vivo

In assessing the biocompatibility of pDA/KAE@ZIF-8 NPs for in vivo applications, a key factor to consider is their hemolysis rate when interacting with blood. Figure 9A displays the results of a hemolysis test, which involved exposing various concentrations of NPs to an erythrocyte suspension for 3 hours. In this experiment, PBS and pure water were used as negative and positive controls, respectively. The results were encouraging: at all tested concentrations, pDA/ KAE@ZIF-8 NPs caused no visible red color change, and their hemolysis rate was consistently below 5%. This low rate suggests excellent biocompatibility, an essential attribute for biological applications.

To further evaluate biocompatibility, we conducted a comparative analysis involving routine blood tests, liver and kidney function assessments, and H&E staining of vital organs (heart, liver, spleen, lung, kidney, and brain). This
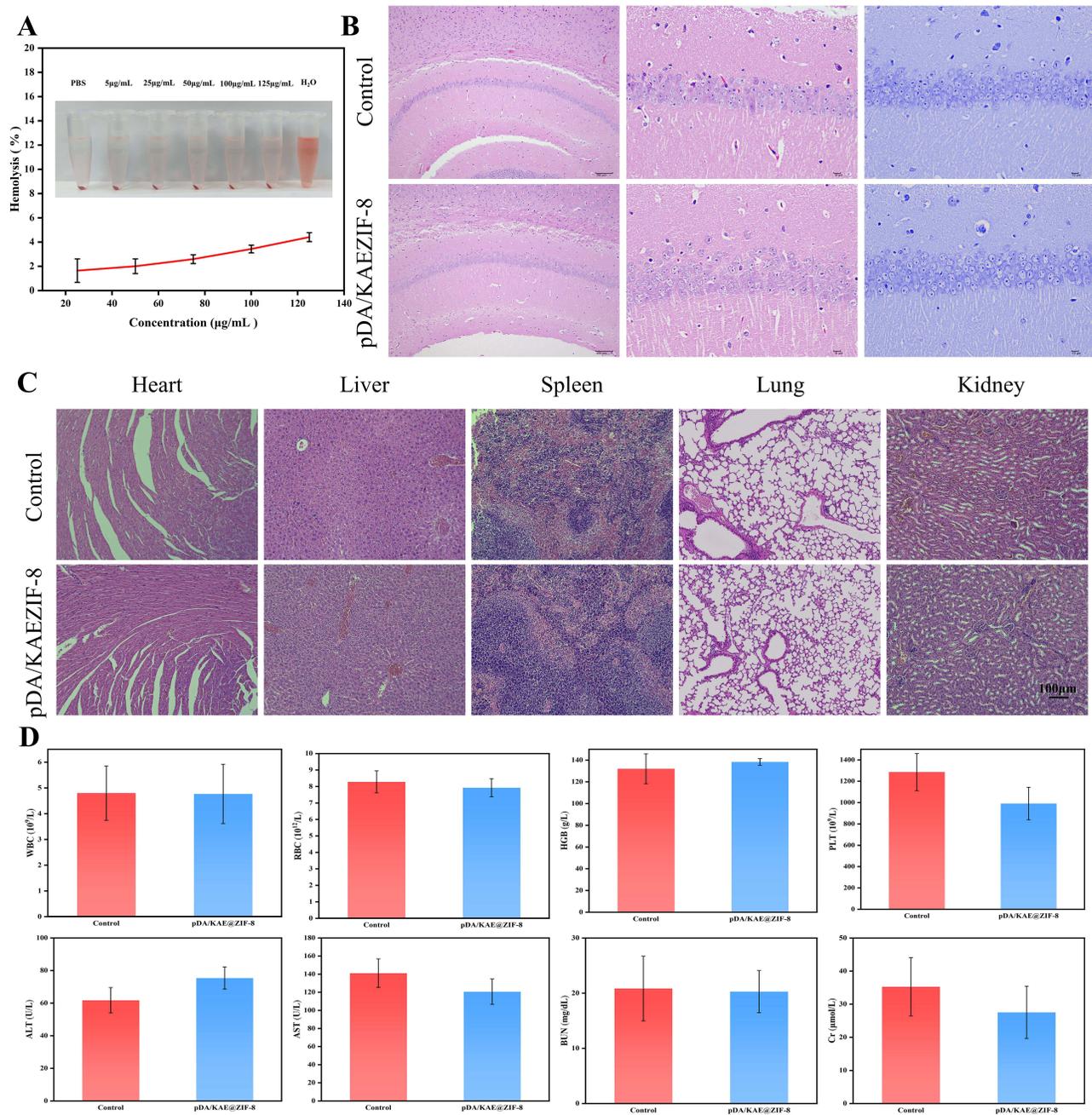
Figure 9 The in vivo biocompatibility of pDA/KAE@ZIF-8 NPs. (**A**) Assessment of hemolysis rates at varying concentrations of NPs. (**B**) Examination of NPs' impact on murine brain tissue in both treated and normal mice through H&E and Nissl staining. (**C**) HE staining of heart, liver, spleen, lung, and kidney tissues in mice subjected to NPs treatment compared to normal mice. (**D**) Comprehensive evaluation of hematological parameters and hepatic and renal function in mice following NPs treatment in comparison to normal mice.

comparison was made between normal mice and mice injected with NPs, as shown in Figures 9B-D. Importantly, no significant cell damage or apoptosis was detected in the major organs of mice treated with NPs. This finding indicates that the treatment with pDA/KAE@ZIF-8 NPs did not induce any toxic side effects in the mice.

The combination of the low hemolysis rate and the absence of toxicological effects in major organs strongly supports the potential of pDA/KAE@ZIF-8 NPs for targeted PND therapy. Their good biocompatibility makes them a promising candidate for further development and application in this field.

Discussion

This study introduces an innovative nanomedicine approach for PND treatment, featuring polydopamine-modified ZIF-8 nanoparticles loaded with KAE. These nanoparticles effectively penetrate the BBB, alleviating oxidative stress, reducing inflammation and neuronal apoptosis, and significantly enhancing cognitive function in a PND mouse model. PND, a common postoperative complication in elderly patients, particularly affects those over 65 years old, with an incidence rate of 25.8–41.4% in general surgery and beyond 50% in cardiac surgery.[29,30] Its symptoms include attention deficits, disordered consciousness, cognitive dysfunction, disturbances in sleep-wake cycles, neuromotor abnormalities, and emotional dysregulation. The lack of effective PND treatments underscores the clinical importance of this study, which not only proposes a novel therapeutic strategy but also addresses the limitations of the traditional drug KAE in terms of bioavailability and solubility. By utilizing a nanomedicine delivery system, the drug's targeting capability and therapeutic efficacy are significantly enhanced. The successful development of pDA/KAE@ZIF-8 NPs opens new avenues in neuroprotective drug design and development. This study stands out by focusing on the application of nanotechnology in PND treatment, extending beyond the scope of previous studies which have explored nanotechnology for drug delivery. We employed network pharmacology to investigate KAE's mechanisms in PND treatment, analyzing multiple targets from extensive experimental and clinical data. This method, known for its scientific reliability, improves the accuracy and credibility of results, guiding drug development and clinical applications.[31] The key aspect of this study was the synthesis and characterization of pDA/KAE@ZIF-8 NPs. Using techniques like SEM, FTIR, XRD, and UV-Vis spectroscopy, we confirmed their successful synthesis and unique chemical and physical properties. Compared to existing nanomedicine research, pDA/KAE@ZIF-8NPs demonstrated superior biocompatibility and targeting, along with outstanding ROS scavenging capabilities and stability under physiological conditions.[32–34] The immune escape capability of PDA shell nanoparticles primarily stems from their unique surface chemical properties, which can reduce recognition and reaction by the immune system. Numerous in vitro and in vivo studies[35–38] have indicated that the core-shell structure of PDA coatings enhances the biocompatibility and modifiability of the materials. PDA itself contains various functional groups, which can react with drugs, biomolecules, or polymers, thereby enhancing the biocompatibility and dispersibility of nanoparticles and reducing the activation of the immune system. Additionally, by mimicking the surface properties of biocompatible materials, the PDA shell can reduce the adsorption of non-specific proteins on the surface of nanoparticles, thereby decreasing the likelihood of recognition and clearance by macrophages. These mechanisms work together to provide PDA-encapsulated nanoparticles with better circulatory stability and a longer half-life in the body, thus enhancing the efficiency of drug delivery. These properties are crucial for PND treatment, echoing the findings of Li Changjiang, which emphasized nanoparticles' potential in neuroprotection.[39]

The hippocampus, crucial for cognitive functions, particularly spatial learning and memory, becomes adversely affected when its microglia release pro-inflammatory cytokines (eg, IL-1β, IL-6, TNF-α), ROS, and NO, leading to neuronal dysfunction and cell death.[40,41] Network pharmacology screening identified that KAE targets pathways linked to inflammation and immune regulation, such as the AGE-RAGE signaling pathway,[42] TNF-α signaling pathway,[43] and apoptosis,[44] playing a vital role in neuroprotection and cognitive improvement in PND treatment.[45] In vivo models revealed that pDA/KAE@ZIF-8 NPs significantly impact microglial activation and inflammation, suggesting their potential neuroprotective effects. They inhibit H_2O_2-induced neuroinflammation and oxidative stress, particularly suppressing pathological microglial activation and pro-inflammatory factor secretion. This discovery opens a new perspective on regulating neuroinflammation by modifying microglial activity, potentially influencing the progression of neurodegenerative diseases. Moreover, pDA/KAE@ZIF-8 NPs notably reduce H_2O_2-induced apoptosis in HT-22 hippocampal neurons, providing direct evidence of their neuroprotective effect. The relationship between this effect and microglial influence requires further exploration.

While the mouse PND model yielded positive results, broader validation in other animal models and human clinical trials is essential. Additionally, the long-term biocompatibility, potential toxicity, and behavior of these nanoparticles in complex biological systems warrant further investigation. In summary, pDA/KAE@ZIF-8 NPs, as a novel nanotargeting strategy, show great promise in PND treatment. Their successful synthesis and characterization lay a crucial foundation for future PND research. Despite facing challenges, this innovative approach offers new hope in improving the quality of life for PND patients.

Conclusion

The findings from this study underscore the potential of pDA/KAE@ZIF-8 NPs as an effective nanotherapeutic agent for PND. This approach offers a novel direction in the postoperative care of elderly patients, with the potential to transform the therapeutic landscape for neurocognitive disorders following surgery. The application of nanotechnology in this context opens new avenues for more effective and targeted treatments, thereby improving the quality of life for patients suffering from PND.

Acknowledgments

Disclosure

The authors report no conflicts of interest in this work.

References

1. Needham MJ, Webb CE, Bryden DC. Postoperative cognitive dysfunction and dementia: what we need to know and do. *Br J Anaesth*. 2017;119 (suppl_1):i115–i125. doi:10.1093/bja/aex354
2. Lyashenko EA, Ivanova LG, Chimagomedova AS. [Postoperative cognitive disorder]. *Zh Nevrol Psikhiatr Im S S Korsakova*. 2020;120(10. Vyp. 2):39–45 Russian. doi:10.17116/jnevro202012010239
3. Tasbihgou SR, Absalom AR. Postoperative neurocognitive disorders. *Korean J Anesthesiol*. 2021;74(1):15–22. doi:10.4097/kja.20294
4. Zhang Q, Wu Y, Han T, Liu E. Changes in cognitive function and risk factors for cognitive impairment of the elderly in China: 2005–2014. *Int J Environ Res Public Health*. 2019;1616:10.3390/ijerph16162847
5. Wang W, Ma Y, Liu Y, Wang P, Liu Y. Effects of dexmedetomidine anesthesia on early postoperative cognitive dysfunction in elderly patients. *ACS Chem Neurosci*. 2022;13(15):2309–2314. doi:10.1021/acschemneuro.2c00173
6. Lin X, Chen Y, Zhang P, Chen G, Zhou Y, Yu X. The potential mechanism of postoperative cognitive dysfunction in older people. *Exp Gerontol*. 2020;130:110791. doi:10.1016/j.exger.2019.110791
7. Luo A, Yan J, Tang X, Zhao Y, Zhou B, Li S. Postoperative cognitive dysfunction in the aged: the collision of neuroinflammaging with perioperative neuroinflammation. *Inflammopharmacology*. 2019;27(1):27–37. doi:10.1007/s10787-018-00559-0
8. Wang J, Fröhlich H, Torres FB, et al. Mitochondrial dysfunction and oxidative stress contribute to cognitive and motor impairment in FOXP1 syndrome. *Proc Natl Acad Sci U S A*. 2022;119(8):1.
9. Haugh AM, Probasco JC, Johnson DB. Neurologic complications of immune checkpoint inhibitors. *Expert Opin Drug Saf*. 2020;19(4):479–488. doi:10.1080/14740338.2020.1738382
10. Fonken LK, Frank MG, D'Angelo HM, et al. Mycobacterium vaccae immunization protects aged rats from surgery-elicited neuroinflammation and cognitive dysfunction. *Neurobiol Aging*. 2018;71:105–114. doi:10.1016/j.neurobiolaging.2018.07.012
11. Abramov AY. Redox biology in neurodegenerative disorders. *Free Radic Biol Med*. 2022. 188;24–25. doi:10.1016/j.freeradbiomed.2022.06.229
12. Yang Q, Li M, Liu J, et al. Intermittent fasting ameliorates neuronal ferroptosis and cognitive impairment in mice after traumatic brain injury. *Nutrition*. 2023. 109. 111992. 10.1016/j.nut.2023.111992
13. Feng C, Jiang Y, Li S, et al. Methionine restriction improves cognitive ability by alleviating hippocampal neuronal apoptosis through H19 in middle-aged insulin-resistant mice. *Nutrients*. 2022;14(21):4503. doi:10.3390/nu14214503
14. Yang J, Sun P, Xu X, et al. TAK1 improves cognitive function via suppressing RIPK1-driven neuronal apoptosis and necroptosis in rats with chronic hypertension. *Aging Dis*. 2023. doi:10.14336/ad.2023.0219
15. Yang C, Yang W, He Z, et al. Kaempferol improves lung ischemia-reperfusion injury via antiinflammation and antioxidative stress regulated by SIRT1/HMGB1/NF-κB axis. *Front Pharmacol*. 2019;10:1635. doi:10.3389/fphar.2019.01635
16. Alam W, Khan H, Shah MA, Cauli O, Saso L. Kaempferol as a Dietary Anti-inflammatory agent: current therapeutic standing. *Molecules*. 2020;25 (18):4073. doi:10.3390/molecules25184073
17. Park SE, Sapkota K, Kim S, Kim H, Kim SJ. Kaempferol acts through mitogen-activated protein kinases and protein kinase B/AKT to elicit protection in a model of neuroinflammation in BV2 microglial cells. *Br J Pharmacol*. 2011;164(3):1008–1025. doi:10.1111/j.1476-5381.2011.01389.x
18. Liu Z, Yao X, Sun B, et al. Pretreatment with kaempferol attenuates microglia-mediate neuroinflammation by inhibiting MAPKs-NF-κB signaling pathway and pyroptosis after secondary spinal cord injury. *Free Radic Biol Med*. 2021. 168. 142–154. 10.1016/j.freeradbiomed.2021.03.037
19. Xie H, Liu X, Huang Z, et al. Nanoscale Zeolitic Imidazolate Framework (ZIF)-8 in cancer theranostics: current challenges and prospects. *Cancers*. 2022;14(16):3935. doi:10.3390/cancers14163935
20. He L, Huang G, Liu H, Sang C, Liu X, Chen T. Highly bioactive zeolitic imidazolate framework-8-capped nanotherapeutics for efficient reversal of reperfusion-induced injury in ischemic stroke. *Sci Adv*. 2020;6(12):eaay9751. doi:10.1126/sciadv.aay9751
21. Liu X, Jansman MMT, Li W, Kempen P, Thulstrup PW, Hosta-Rigau L. Metal-organic framework-based oxygen carriers with antioxidant protection as a result of a polydopamine coating. *Biomater Sci*. 2021;9(21):7257–7274. doi:10.1039/d1bm01005k
22. Qi D, Lin H, Hu B, Wei Y. A review on in vitro model of the blood-brain barrier (BBB) based on hCMEC/D3 cells. *J Control Release*. 2023; 358:78–97. 10.1016/j.jconrel.2023.04.020

23. Ouyang Y, Su X, Zheng X, et al. Mussel-inspired "all-in-one" sodium alginate/carboxymethyl chitosan hydrogel patch promotes healing of infected wound. *Int J Biol Macromol*. 2024;261(Pt 2):129828. 10.1016/j.ijbiomac.2024.129828.

24. Gao P, Chang K, Yuan S, et al. Exploring the mechanism of hepatotoxicity induced by dictamnus dasycarpus based on network pharmacology, molecular docking and experimental pharmacology. *Molecules*. 2023;28(13):5045. doi:10.3390/molecules28135045

25. Yin X, Ran S, Cheng H, et al. Polydopamine-modified ZIF-8 nanoparticles as a drug carrier for combined chemo-photothermal osteosarcoma therapy. *Colloids Surf B Biointerfaces*. 2022;216:112507. doi:10.1016/j.colsurfb.2022.112507

26. LWC H, Liu Y, Han R, Bai Q, Choi CHJ. Nano-cell interactions of non-cationic bionanomaterials. *Acc Chem Res*. 2019;52(6):1519–1530. doi:10.1021/acs.accounts.9b00103

27. Seo MK, Jeong S, Seog DH, et al. Effects of liraglutide on depressive behavior in a mouse depression model and cognition in the probe trial of Morris water maze test. *J Affect Disord*. 2022;324:8–15. doi:10.1016/j.jad.2022.12.089

28. Fujita Y, Yamashita T. Mechanisms and significance of microglia-axon interactions in physiological and pathophysiological conditions. *Cell Mol Life Sci*. 2021;78(8):3907–3919. doi:10.1007/s00018-021-03758-1

29. Shen Y, Li X, Yao J. Develop a clinical prediction model for postoperative cognitive dysfunction after major noncardiac surgery in elderly patients: a protocol for a prospective observational study. *Gerontology*. 2022;68(5):538–545. doi:10.1159/000517511

30. Liang Y, Xin X, Wang H, et al. A novel predictive strategy for the incidence of postoperative neurocognitive dysfunction in elderly patients with mild cognitive impairment. *Front Aging Neurosci*. 2022;14:985406. doi:10.3389/fnagi.2022.985406

31. Zhao L, Zhang H, Li N, et al. Network pharmacology, a promising approach to reveal the pharmacology mechanism of Chinese medicine formula. *J Ethnopharmacol*. 2023. 309. 116306. 10.1016/j.jep.2023.116306

32. Pinheiro RGR, Coutinho AJ, Pinheiro M, Neves AR. Nanoparticles for targeted brain drug delivery: what do we know? *Int J Mol Sci*, 2021 22 21 11654 doi: 10.3390/ijms222111654.

33. Zhu Q, Huang Y, Zhu X, et al. Mannose-coated superparamagnetic iron oxide nanozyme for preventing postoperative cognitive dysfunction. *Mater Today Bio Apr*. 2023;19:100568. doi:10.1016/j.mtbio.2023.100568

34. Zhu Y, Zhang J, Li C, et al. Porous Se@SiO(2) nanoparticles attenuate radiation-induced cognitive dysfunction via modulating reactive oxygen species. *ACS Biomater Sci Eng*. 2022;8(3):1342–1353. 10.1021/acsbiomaterials.1c01571.

35. Pi W, Zhang Y, Li L, et al. Polydopamine-coated polycaprolactone/carbon nanotube fibrous scaffolds loaded with brain-derived neurotrophic factor for peripheral nerve regeneration. *Biofabrication*. 2022;14(3):035006. doi:10.1088/1758-5090/ac57a6

36. Wu M, Hong C, Shen C, et al. Polydopamine nanomaterials and their potential applications in the treatment of autoimmune diseases. *Drug Deliv*. 2023;30(1):2289846. doi:10.1080/10717544.2023.2289846

37. Zhang Y, Ren X, Wang Y, et al. Targeting ferroptosis by polydopamine nanoparticles protects heart against ischemia/reperfusion injury. *ACS Appl Mater Interfaces*. 2021;13(45):53671–53682. 10.1021/acsami.1c18061.

38. Fu Y, Yang L, Zhang J, et al. Polydopamine antibacterial materials. *Mater Horiz*. 2021;8(6):1618–1633. 10.1039/d0mh01985b.

39. Li C, Wang N, Zheng G, Yang L. Oral administration of resveratrol-selenium-peptide nanocomposites alleviates alzheimer's disease-like pathogenesis by inhibiting aβ aggregation and regulating gut microbiota. *ACS Appl Mater Interfaces*. 2021;13(39):46406–46420. doi:10.1021/acsami.1c14818

40. Cho J, Pavlides C. Hippocampal cellular functional organization for fear memory: effects of sleep. *Hippocampus*. 2022;32(11–12):839–856. doi:10.1002/hipo.23477

41. Du Y, Brennan FH, Popovich PG, Zhou M. Microglia maintain the normal structure and function of the hippocampal astrocyte network. *Glia*. 2022;70(7):1359–1379. doi:10.1002/glia.24179

42. Chen C, Li XH, Tu Y, et al. Aβ-AGE aggravates cognitive deficit in rats via RAGE pathway. *Neuroscience*. 2014. 257. 1–10. 10.1016/j.neuroscience.2013.10.056

43. Yin S, Ma XY, Sun YF, et al. RGS5 augments astrocyte activation and facilitates neuroinflammation via TNF signaling. *J Neuroinflammation*. 2023;20(1):203. 10.1186/s12974-023-02884-w.

44. Mani V, Alshammeri BS. Quetiapine moderates doxorubicin-induced cognitive deficits: influence of oxidative stress, neuroinflammation, and cellular apoptosis. *Int J Mol Sci*, 2023 24 14 11525 doi: 10.3390/ijms241411525.

45. Chai WN, Wu YF, Wu ZM, et al. Neat1 decreases neuronal apoptosis after oxygen and glucose deprivation. *Neural Regen Res*. 2022;17(1):163–169. doi:10.4103/1673-5374.314313